

Anisotropy in Pulsar Interstellar Scattering

Barney Rickett *

Department of Electrical & Computer Engineering
University of California, San Diego, CA92093-0407

Abstract Pulsar observers have to contend with several effects of propagation through the ionized interstellar medium. I review those effects and how they can be used to study the interstellar plasma. Pulsars are normally observed under conditions of strong scintillation and show both diffractive and refractive effects. I emphasize the diffractive scintillation as exhibited in the dynamic spectrum and in its converse – pulse broadening. From Parkes observations of the pulse broadening of PSR J1644–45, I estimate the inner scale in an interstellar region of strong plasma turbulence to be about 100 km. I discuss the representation of dynamic spectra in terms of their “secondary spectra” and show how the arcs, that are often revealed, are related to both angular broadening and pulse broadening. Anisotropy in the scattering both changes the scattered pulse shape but also enhances the visibility of the arcs.

Key words: pulsars—turbulence—scattering—interstellar medium

1 INTERSTELLAR DISPERSION AND SCATTERING

The starting point for analysis of interstellar propagation effects for pulsars is the dispersion of pulse arrival time versus frequency. From the change in arrival time observed over a bandwidth $\delta\nu$ centered at frequency (ν_0), we can determine the dispersion measure DM, which is the column density of electrons along the path L from each pulsar. One can also think of the corresponding radio propagation phase over that path $\phi = (2\pi/\lambda) \int_0^L n(\mathbf{r}z/L, z) dz$, where $n(\mathbf{r}, z)$ is the refractive index at transverse position \mathbf{r} and distance z from the pulsar. Assuming that the interstellar electron density N_e is such that ν_0 is always much larger than the local plasma frequency, we obtain $\phi = L(2\pi\nu_0/c) + r_e DM \lambda$, where $r_e = 2.82 \times 10^{-15}$ m is the classical electron radius. The associated group delay $T_g = \partial\phi/\partial\nu/(2\pi) = L/c + r_e DM/(2\pi\nu_0^2)$; subtracting the free-space terms, we see that the dispersive plasma delay is simply related to the plasma phase as $T_g = -\phi/(2\pi\nu_0)$ (Rickett 1988). Of course, pulsar observers have to remove the differential delay that this causes over the bandwidth, either by coherent or incoherent methods.

The best timing measurements require correction for changes in DM, as was done by Kaspi et al. (1994) for early measurements of PSR B1937+21. Ramachandran et al. (2006) have recently assembled 20 years of timing results on this pulsar at various radio frequencies, from which they have estimated the variations in DM and its structure function. Because of the relation of plasma delay to plasma phase one can directly obtain the structure function in ϕ (their figure 7). At 1.4 GHz they fit it by the function:

$$D_\phi(t) = \langle [\phi(t') - \phi(t' + t)]^2 \rangle = (t/\delta t_d)^\alpha \text{ [radian}^2\text{]}, \quad (1)$$

over times from 12–5000 days and estimate $\delta t_d = 180$ s and $\alpha = 1.66$ consistent with $5/3$, as expected for a medium with a Kolmogorov wavenumber spectrum. The changes in DM or ϕ are largely due to the motion of the line of sight from the pulsar to the Earth relative to the dispersing interstellar electrons. Ramachandran et al. estimate this velocity to be 40 km s^{-1} for mapping time scales to spatial scales. Hence the spatial scale associated with δt_d is 7200 km. The same transverse gradients in ϕ that cause DM to vary also cause interstellar scattering and scintillation (ISS). In pulsars the primary effects are broadening of the pulse shape and fluctuations in the pulse amplitude over time and frequency.

* E-mail: bjrickett@ucsd.edu

Interstellar Scattering

Considering the scintillation first, the dominant (diffractive) scale (s_d) is defined by the separation where the spatial structure function equals one radian². When the scattering medium can be described by an isotropic Kolmogorov wavenumber spectrum we obtain $D_\phi(b) = (b/s_d)^{5/3}$. If the spectrum were anisotropic with an axial ratio A , D_ϕ is a similar power law of the quadratic form $\sqrt{A(x/s_d)^2 + (y/s_d)^2}/A$. The diffractive scale is intimately linked to the angular broadening angle $\theta_d = \lambda/(2\pi s_d)$, which is the characteristic width of the angular spectrum for plane incident wave. Thus smaller diffractive scales correspond to wider angular scattering and vice-versa; and so anisotropy causes wider scattering in the spatially narrow direction (here x). For the pulsar geometry we have a point source at distance L and if the scattering occurs in a relatively thin layer at distance sL from the pulsar, the apparent angles of arrival at the observer would be $\theta_2 = s\theta_d$.

The mutual interference of the waves scattered at different angles causes the intensity to vary across a wavefront and then the motion of the observer relative to the pulsar and medium cause variations in time (Interstellar Scintillation - ISS). In pulsar observations we normally have “strong scintillation” which is when $m = (I_{\text{rms}}/I) > 1$, and the dominant effect is diffractive intensity fluctuations over a scale s_d with a scintillation index $m \sim 1$. Actual measurements of the diffractive ISS of PSR B1937+21 at 1.4 GHz by Cordes et al. (1990) showed a scale of 17800 km. This can be compared with the 7200 km which was extrapolated over a factor of 2300:1 from the DM variations. The difference suggests an exponent slightly steeper than the fitted value of 1.66 – perhaps due to the effect of an inner scale.

As is well known diffractive ISS is a narrow band process, which is characterized by the frequency difference for a 50% decorrelation in the ISS ($\delta\nu_d$). There are also refractive interstellar scintillations (RISS) which occur on time-scales of days to months, corresponding to scales in the medium on the size of the scattering disk, which are typically correlated over a 2:1 bandwidth. The latter have rms amplitudes of 1%–20% and will not be discussed further.

Temporal and Angular Broadening

Interstellar pulse broadening is also due to diffraction. The extra path length for a wave component deflected by the screen through an angle θ_s causes a time delay $t = z_e\theta_s^2/(2c)$ where $z_e = Ls(1-s)$ with s as the pulsar-screen distance as a fraction of the pulsar-earth distance. The pulse broadening is also related to the narrow band diffractive ISS, having a characteristic decay time $\tau_d \sim (2\pi\delta\nu_d)^{-1}$. The scattered pulse shape is related directly to the angular scattering spectrum ($B(\theta_s, \beta)$) as $P(t) = \int_0^{2\pi} B(\theta_s = \sqrt{(2ct/z_e), \beta})d\beta$, where β is the “azimuth” of θ_s . In almost all discussions of this pulse broadening the scattering has been assumed to be isotropic making the β integration unimportant. Figure 1 shows a simple calculation of the effect of anisotropy using an elliptical Gaussian angular scattering function with axial ratio $A = 1, 2, 4, 8$. As is well-known, the circularly symmetric case ($A = 1$) maps the Gaussian brightness distribution to a one-sided exponential pulse shape, which is a straight line on the \log_e -linear scale. As A increases, the far-out pulse decay becomes slower (due to the late arrival of waves scattered in the wide direction). Thus high dynamic range measurements of the scattered pulse shape can be influenced by anisotropy in the scattering.

Pulse Broadening as a Probe of Interstellar Scattering

The effect of anisotropy is a serious complication in the interpretation of the detailed form of the far-out pulse decay, as a probe for an inner scale in the scattering plasma. Figure 2 shows observations by Rickett et al. (2005) of the pulse decay at 660 MHz from PSR J1644–45 (observed at Parkes for an hour using 1024 channels over a bandwidth of 32 MHz). The data were fitted by a theoretical model with **isotropic** Kolmogorov scattering with an inner scale from either a screen (on left) or an extended medium (on right). The model was fitted to the pulse decay (from the thin dotted line onwards) to avoid the influence of the intrinsic pulse shape. The fitted parameters were the diffractive time constant, the inner scale and the off-pulse level of the received power. The solid lines are the best fit Kolmogorov spectrum models; the error bars show the observed pulse relative to the base level, which was estimated independently for the two models. The dotted line is for a large inner scale (exponential decay) and the dashed line is for a small inner scale (simple Kolmogorov) model with the fitted time constants. The fact that the observations lie between

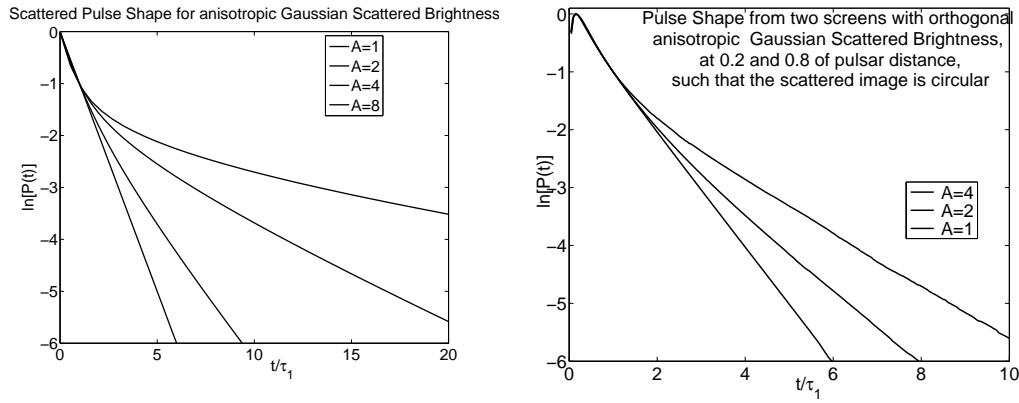


Fig. 1 (a) *Left*: Pulse shape due to screen with elliptical Gaussian Scattered brightness functions. Vertical scale is natural log of scattered pulse response. Axial ratios $A = 1, 2, 4, \& 8$ (from lowest to highest curve). (b) *Right*: Pulse shape due to two screens with orthogonal scattering ellipses of axial ratios as listed; the configuration is constrained so that the apparent scattered image is circular.

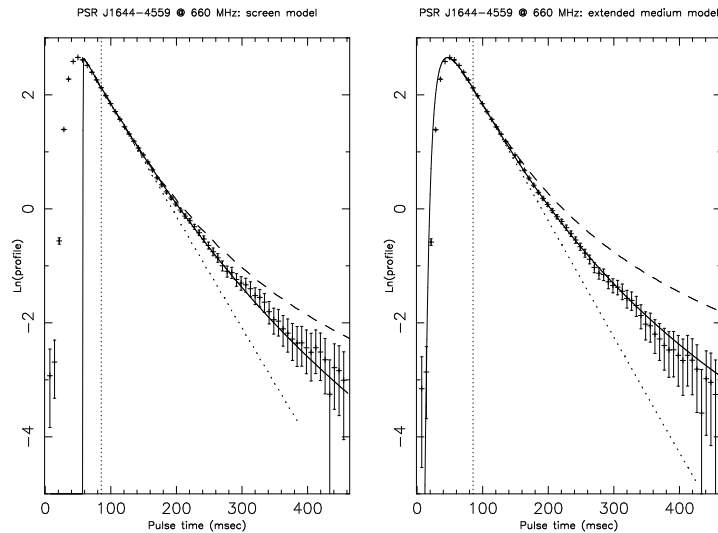


Fig. 2 Natural log of the observed pulse profile averaged over 32 MHz near 660 MHz; screen (left) and extended medium (right) model fits are overplotted. Parkes observations by Rickett et al. (2005).

these two extremes allows us to estimate the inner scale. The estimated inner scale is 76 ± 5 km for the extended scattering medium, while it is $(190 \pm 12)\sqrt{s(1-s)}$ km for a screen at fractional distance s .

We saw in Figure 1a that the effect of anisotropy in a screen is to cause a slower pulse decay at late times (curving upwards relative to the straight line). Though this calculation was for a very large inner scale (Gaussian scattered brightness), we expect a similar effect for the Kolmogorov models. An unknown axial ratio would cause a degeneracy in the fit and so the quoted inner scale results become lower bounds if the axial ratio is larger than 1.5.

We do not have a theoretical pulse shape for an extended medium with anisotropic scattering. Of course such a model would also have to specify how the orientation of the major axis of the scattering varies with

distance. As a simple test of the physical ideas involved, we computed the pulse shape due to scattering in two orthogonal elliptical Gaussian screens (see Figure 1b). The screens are at 0.2 and 0.8 of the pulsar distance and their scattering ellipses had equal axial ratios with their angles of scattering constrained so that the overall scattered image appears to be circular for the observer. The point of interest here is that the pulse shape, which would be exponential for a single circular Gaussian screen, has a slower late-time decay as the axial ratio increases. This is because angular broadening and temporal broadening have differing weighting functions versus distance. Screens near the pulsar have a bigger effect on the pulse decay than on the apparent scattering angle and vice versa. We anticipate that some traces of this behaviour would be seen in the pulse shape from an extended distribution of randomly oriented scattering ellipses. The equations used are:

$$P(t) = \iint B_1(\boldsymbol{\theta}_{s1})B_2(\boldsymbol{\theta}_{s2})\delta[t - \tau(\boldsymbol{\theta}_{s1}, \boldsymbol{\theta}_{s2})]d\boldsymbol{\theta}_{s1}d\boldsymbol{\theta}_{s2}, \quad (2)$$

where

$$\tau(\boldsymbol{\theta}_{s1}, \boldsymbol{\theta}_{s2}) = [(L - z_1)z_2\theta_{s1}^2 + z_2(L - z_1)\theta_{s2}^2 + 2z_2(L - z_1)\boldsymbol{\theta}_{s1}\boldsymbol{\theta}_{s2}]/(2cL). \quad (3)$$

Here z_1 and z_2 are the distances from each screen to the observer which for Figure 1b are $0.2L$ and $0.8L$.

2 DYNAMIC SPECTRA, SECONDARY SPECTRA AND ARCS

The usual display of diffractive ISS is the dynamic spectrum, (as in Figure 3) which plots pulse intensity versus frequency and time. The intensity is usually estimated from the area of average pulse profiles observed in a channel bandwidth $\delta\nu$ integrated for time δt . A striking feature of such plots is that the intensity is deeply modulated in frequency ($\delta\nu_d$) as well as in time (δt_d). The condition to see the ISS is evidently that the channel bandwidth is narrower than the characteristic scintillation bandwidth $\delta\nu_d$ and also $\delta t < \delta t_d$. In contrast, the condition to see pulse broadening is that the basic time resolution $\sim (2\delta\nu)^{-1}$ is smaller than the pulse decay time τ_d , or equivalently the observed channel bandwidth includes many independent scintles (if dispersion is removed coherently then one needs many diffractive scintles across the total bandwidth).

The left panel of Figure 3 shows the primary dynamic spectrum. One can recognize the characteristic widths ($\delta\nu_d \times \delta t_d$), but with sufficiently fine resolutions one can also see a criss-cross patterned substructure. The right panel shows its Fourier power spectrum (secondary spectrum) plotted logarithmically versus delay f_ν (μs) and frequency f_t (MHz). The parabolic arcs (first discovered by Stinebring et al. 2001) extend well beyond τ_d in delay. The relationships between the scattered pulse shape, scattered brightness distribution, primary dynamic spectrum and secondary spectrum are summarized in Figure 4, which also illustrates how these quantities are related to the generalized second moment of the received electric field ($\Gamma_{2D}(\boldsymbol{\sigma}, \delta\nu)$). Note that the sum of S_2 over f_t gives the auto-correlation ($R_P(\delta t)$) of the scattered pulse shape.

However, the relationships in Figure 4 do not explain the physics of the parabolic arcs, which is due to interference of pairs of components in the scattered brightness at $\boldsymbol{\theta}_{s1}$ and $\boldsymbol{\theta}_{s2}$ (see Stinebring et al. 2001; Cordes et al. 2006; Walker et al. 2004). The components have differing delays and differing Doppler shifts due to their changing path lengths. While the delay depends on the square of the angles ($z_e\theta_s^2/2c$), the difference in Doppler shifts depends linearly on the angles, giving $f_t = \mathbf{V} \cdot (\boldsymbol{\theta}_{s1} - \boldsymbol{\theta}_{s2})/(\lambda)$, where \mathbf{V} is the ‘‘scintillation velocity’’ relative to the medium. These linear and quadratic dependencies give a general quadratic relation between f_t and f_ν .

In the special case that one of the angles is close to zero and $\boldsymbol{\theta}_{s1} = (\theta_{sx1}, \theta_{sy1})$, the quadratic becomes a parabola $f_\nu = af_t^2 + b$, where $a = z_e\lambda^2/(2cV^2)$. If \mathbf{V} is along the x -axis $b \propto \theta_{sy1}^2$ which is positive, and hence S_2 falls to zero outside the primary arc $f_\nu = af_t^2$. Moreover in such a case, any point (f_ν, f_t) inside that arc can be mapped to the scattered brightness distribution $B(\theta_s, \beta)$, as $\theta_s = \sqrt{(2cf_\nu/z_e)} = (\lambda/V)\sqrt{f_\nu/a}$ and $\cos\beta = f_t\sqrt{a/f_\nu}$. Thus we have the remarkable result that an observation of the secondary spectrum with a single antenna can be mapped to the two dimensional scattered brightness (though since only $\cos\beta$ is determined points at $\pm\beta$ are superimposed).

The mapping is such that S_2 is greatest for waves from near $\beta = 0$ or π , which brightens the outer edge of the arc. It also means that thin bright arcs occur when the scattering is anisotropic and aligned with the velocity. In Figure 3 the most prominent arc is quite narrow as if due to anisotropy, while the arc that lies

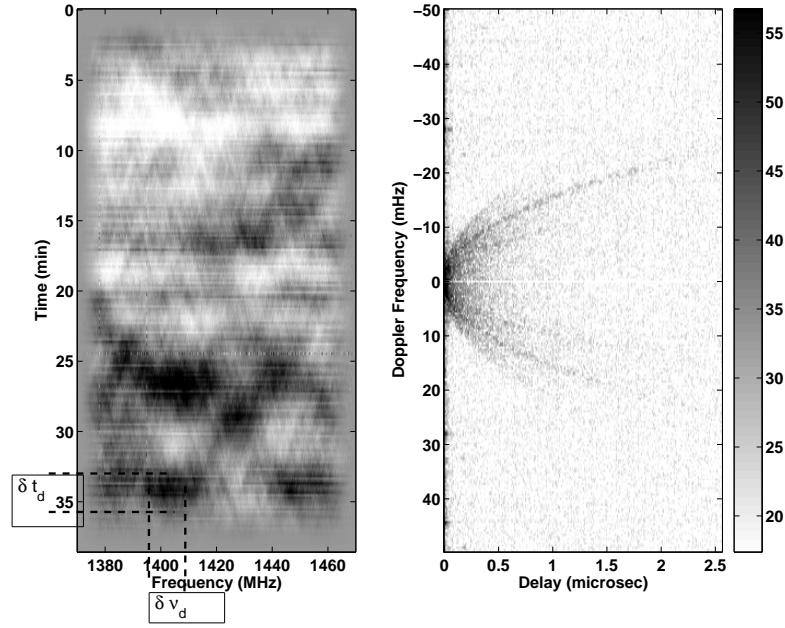


Fig. 3 *Left*: Dynamic spectrum of PSR B1133+16 recorded by Stinebring at Arecibo on modified Julian Date 53224; the darkness of the grayscale is linear in intensity. *Right*: The secondary spectrum (S_2) of the data on the left (its 2-D Fourier power spectrum). The greyscale is logarithmic (dB) as shown in the tablet, revealing remarkable fine parabolic arcs visible out to delays much larger than τ_d , which is the width in delay of the dark region near the origin and can also be estimated as $(2\pi\delta\nu_d)^{-1}$.

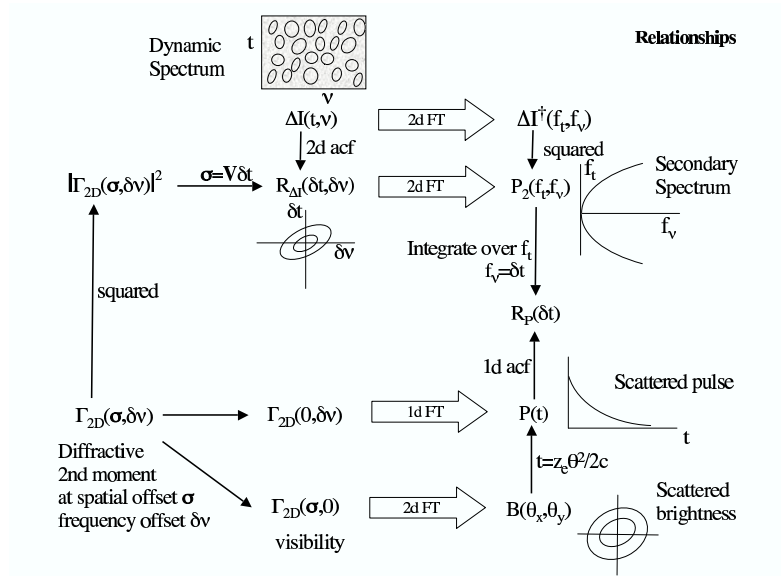


Fig. 4 Relationships between primary, secondary spectra, scattered brightness distribution, pulse shape, and the second moments of the field.

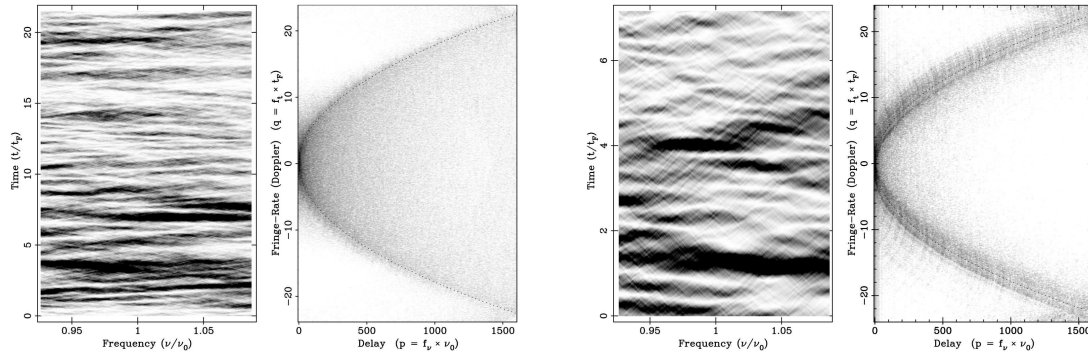


Fig. 5 Simulated primary and secondary spectrum for a Kolmogorov screen in intermediate scintillation. *Left:* Axial ratio = 1.0; *Right:* Axial ratio 4:1. The strength of scintillation as characterized by the variance calculated assuming weak scintillation (ie the Born model) was 10.

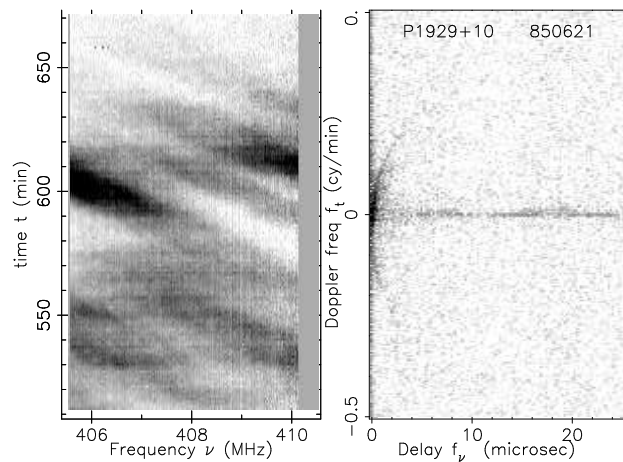


Fig. 6 408 MHz Secondary spectrum from PSR B1929+10 observed at Jodrell Bank 1985 June 21. The slopes are caused by refraction which also shifts the apex of the parabola.

outside it has a filled interior, suggesting a more isotropic scattering at its distance (presumably nearer to the pulsar).

The special case of a strong undeviated component arises directly in weak scintillation, where there is an essentially unscattered “core” that interferes with the scattered waves. The other case is in strong scintillation from a medium with a power law spectrum (like the Kolmogorov spectrum); then waves within the half-power width of the ensemble averaged scattered brightness act as the core and interfere with an effective “halo” of waves from much higher angles. The mapping described above is robust in weak scintillation but only applies in strong scintillation under conditions that approach an ensemble average, and then the effective resolution is set by the scattered core. This is distinct from the inversion technique of Walker and Stinebring (2005), who attempt to estimate B under snapshot conditions.

Cordes et al. (2006) describe the theory of arcs under asymptotic weak and strong scintillation; they also present simulations for some intermediate cases, which are reproduced in Figure 5. Both left and

right panels are for Kolmogorov spectra with the same strength of scintillation, but the left is isotropic and the right is anisotropic with an axial ratio 4:1 aligned with wider angular scattering along the velocity. These verify that arcs can be seen at intermediate strengths of scintillation and are enhanced when there is anisotropy aligned with the velocity.

Figure 6 illustrates the arc phenomenon for a case in which the dynamic spectrum (on left) shows pronounced sloping features. The sloping features are due to refraction by a gradient in electron column density, that shifts the scattered image through an angle (say θ_r), but as is discussed in Cordes et al. (2006) the direction for a minimum group delay (f_ν) is at $-\theta_r$. The observable consequence is that while the arc is brighter for positive Doppler, its apex is at negative Doppler.

3 SUMMARY

I have reviewed some of the basics of interstellar dispersion and scattering and the influence of anisotropic scattering. Anisotropy causes the scattered pulse shape at far-out times to decay more slowly than its initial rate of decay. This is seen as a convex curve when plotted on log/linear scales. The effect complicates attempts to use the shape of the far-out decay to estimate an inner scale to the standard Kolmogorov model for the interstellar density.

I also reviewed the basic cause of parabolic arcs in the secondary spectrum plotted versus the differential delay and the differential Doppler shift between two components of the scattered angular spectrum. The special case in which one of the components follows a nearly straight path leads to the parabolic form often observed. That special condition occurs directly in weak scintillation, and approximately applies under strong scintillation. Anisotropy enhances the visibility of arcs. Plasma refraction shifts the direction for maximum brightness in the opposite direction to that for minimum delay.

Acknowledgements Many of the ideas here were developed jointly with my long-time colleague Bill Coles. I thank him for very many valuable discussions and for pointing out that anisotropy has a strong effect on the scattered pulse shape. This work was partially funded by the US NSF under grants AST 9988398 and 0507713. I also thank Dr. Wang Na for travel support.

References

- Cordes J. M., et al., 1990, ApJ, 349, 245
 Cordes J. M., Rickett B. J., Stinebring D. R., Coles W. A., 2006, ApJ, 637, 346
 Hill A. S., Stinebring D. R., Asplund C. T. et al., 2005, ApJ, 619, L171
 Ramachandran R., Demorest P., Backer D. C. et al., 2006, ApJ, 645, 303
 Rickett B. J., 1988, in "Radio wave Scattering in the Interstellar Medium", Cordes J. M., Rickett B. J., Backer D. C., eds., AIP Conference Proceedings, 174, 2
 Rickett B. J., Johnston S., Tomlinson T., Reynolds J., 2005, MNRAS, preprint
 Stinebring D. R., McLaughlin M. A., Cordes J. M. et al., 2001, ApJ, 549, L97
 Walker M. A., Melrose D. B., Stinebring D. R., Zhang C. M., 2004, MNRAS, 354, 43
 Walker M. A., Stinebring D. R., 2005, MNRAS, 362, 1279